UC San Diego
UC San Diego Previously Published Works

Title
Surface acoustic wave micromotor with arbitrary axis rotational capability

Permalink
https://escholarship.org/uc/item/3qw600jh

Journal
Applied Physics Letters, 99(21)

ISSN
0003-6951

Authors
Tjeung, Ricky T
Hughes, Mark S
Yeo, Leslie Y
et al.

Publication Date
2011-11-21

DOI
10.1063/1.3662931

Peer reviewed

Surface acoustic wave micromotor with arbitrary axis rotational capability

Ricky T. Tjeung, Mark S. Hughes, Leslie Y. Yeo, and James R. Friend[a)]

Micro/Nanophysics Research Laboratory, Melbourne Centre for Nanofabrication and the Department of Mechanical Engineering, Monash University, Clayton, Victoria, Australia

A surface acoustic wave (SAW) actuated rotary motor is reported here, consisting of a millimeter-sized spherical metal rotor placed on the surface of a lead zirconate titanate piezoelectric substrate upon which the SAW is made to propagate. At the design frequency of 3.2 MHz and with a fixed preload of 41.1 μN, the maximum rotational speed and torque achieved were approximately 1900 rpm and 5.37 μN-mm, respectively, producing a maximum output power of 1.19 μW. The surface vibrations were visualized using laser Doppler vibrometry and indicate that the rotational motion arises due to retrograde elliptical motions of the piezoelectric surface elements. Rotation about orthogonal axes in the plane of the substrate has been obtained by using orthogonally placed interdigital electrodes on the substrate to generate SAW impinging on the rotor, offering a means to generate rotation about an arbitrary axis in the plane of the substrate. © *2011 American Institute of Physics*. [doi:10.1063/1.3662931]

Despite many applications in microrobotics and microsurgery[1] and the schemes proposed to generate micromotion, including electrostatic, electromagnetic, and piezoelectric,[2] few practical motors exist at appropriate scales to enable them. The main challenges are the inherent complexity of the final device and the accuracy necessary in fabrication, requiring design simplicity and creativity in machining techniques.[3–7] While the use of bulk flexural waves at small scales has been proposed in the past for ultrasonic piezoelectric micromotors,[8,9] the problem of fabricating piezoelectric thick films with performance characteristics sufficient for actuation[10] has never really been overcome. Surface acoustic waves (SAW), on the other hand, may be generated in thick substrates and offer substantially greater flexibility in mounting and materials choices, not to mention the extraordinary power densities that may be achieved and the benefit that may be drawn from the decades-long effort in using SAW for telecommunications.[11,12]

Most SAW actuators to date have been millimeter-scale, *linear* actuators that use Rayleigh waves traveling across the surface of a piezoelectric material,[5,13,14] usually 127.68° Y-cut *x*-propagating (see Fig. 1 for coordinates) lithium niobate (LN).[15] Rayleigh waves possess in-plane, longitudinal (*x*-axis) motion leading, temporally by one-quarter of a period, transverse (*z*-axis) motions of approximately the same amplitude as they propagate along the *x*-axis. Points of the surface move in retrograde ellipses in the *x*–*z* plane, and an object placed upon the surface will move toward the source of acoustic radiation along the *x*-axis. The maximum speed is determined by the particle or vibration velocity of the wave, around 1 m/s:[5,14] a motor 60×15 mm in size generated up to 18 N force and a speed of 0.9 m/s with 250 V_{p-p} input,[14] but required a preload force of 120 N between the chemically reduced[16] LN substrate and Si slider, unfortunately causing wear that limits the motor's use to a few tens of cycles at most.

SAW motors, where the object in motion rotates about an axis, are far more rare; Cheng *et al.*[17] reports one of two known examples. Rayleigh SAW propagating in opposition from adjacent interdigital electrodes (IDTs) is used to drive a collection of steel balls housed in a 9-mm diameter disc; the disc is allowed to rotate on a hub placed between the counter-propagating SAW, altogether resembling a circus carousel. Probably due to substantial parasitic friction and standing wave SAW at the overlap region between the counter-propagating SAWs, the maximum rotation speed is only 270 rpm and there is no reported torque value, despite a driving voltage of 120 V_{p-p}. A more recent work[18] also makes use of counter-propagating Rayleigh SAW, but with a fluid coupling layer[19] to rotate a 5-mm disc at up to 2250 rpm and with 60 N-m torque. The inconvenience of the fluid common to fluid bearing-driven and acoustic levitation[20] motors is a drawback, however.

Here, we report the development of a dry friction-coupled Rayleigh SAW-driven motor capable of rotating the rotor, a 1 mm solid steel sphere, about a chosen yet arbitrary axis that lies within the plane of the piezoelectric substrate, lead zirconate titanate (PZT, C–203, Fuji Ceramics Corporation, Japan) as illustrated in Fig. 1. PZT was selected due to outright convenience in testing the concept of the motor, its isotropic piezoelectric properties along the substrate plane, and its large electromechanical coupling coefficient,[21] though the concept does work with other, lead-free materials like LN.

Rayleigh SAW of $f = 3.2$ MHz is generated from straight, unapodized 700 μm pitch IDTs patterned along orthogonal axes in 2 -μm-thick Ag on the PZT substrate using standard photolithography, as illustrated in Fig. 1(a). Polydimethylsiloxane was cast in place around the periphery of the 40-mm diameter substrate to prevent acoustic interference from edge reflections. A blind hole with 250 μm diameter was drilled approximately 350 μm deep into the substrate along the SAW propagation pathway (see Figs. 1(b) and 1(c)), upon which the rotor is placed, preventing it from sliding across the substrate and forming a circular contact line. Here, the roughness of PZT can be a factor—the finished surface of the PZT has a roughness of about 1 μm, and so we polished the contact line using a spare rotor to sub-nm

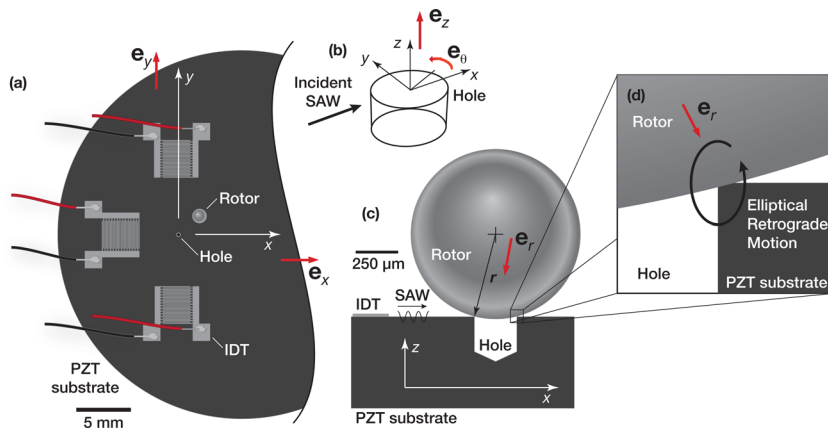[a)]Electronic mail: James.Friend@monash.edu.

FIG. 1. (Color online) (a) Top view of SAW micromotor, a 1 mm solid steel sphere placed atop a retaining hole in PZT patterned with orthogonally placed IDTs. Upon generation of a Rayleigh SAW from an IDT, the SAW propagates (b) past the hole and (c) the contact line formed with the rotor placed upon it. The particle motion is everywhere retrograde with respect to the propagation direction of the SAW, including all points (d) along the contact line. This motion acts against the ball's inertia and generates rotation through stick-slip motion.

roughness before testing. Friction along this contact circle, as the SAW passes, gives rise to rotation.

A laser Doppler vibrometer (LDV; Polytec PI MSA–400, Waldbrunn, Germany) was utilized to visualize the SAW propagation, essentially unaffected by the presence of the hole as shown in Fig. 2, save for a small phase delay of less than 10° and localized amplification of the motion due to stress release of about 15%. These results are expected since the hole diameter and depth are less than the SAW wavelength. The absence of data along path B–B in the hole is due to its sloped bottom preventing reflection of the laser used in LDV measurements.

In contrast to linear SAW motors, rotation can be obtained in this arrangement even with a very small preload force between the rotor and stator only due to gravity—the weight of the rotor, approximately 41.1 μN in our system—because of the large interfacial stress present from the line contact.

The measured z-axis vibration velocity, $\dot{\gamma} = 2\pi f \gamma$, can be used to estimate the maximum rotor velocity, $\omega_{\max}$, generated without placing a load on the rotor. The x-axis, in-plane component of the wave vibration velocity, $\dot{\eta}$, cannot be measured using our LDV but is known to be approximately 70% of the transverse component on the bare surface of hard PZT.[22] Piezoelectric traveling-wave ultrasonic motors rely upon stick-slip mechanisms to generate motion,[23–25] with the local relative motion transverse to the contact locally modulating the friction between the substrate

and rotor. Only recently has it become apparent that bouncing of the rotor can contribute to the dynamics in fascinatingly complex ways,[26] but here, we use an approximate model to estimate its maximum speed. We assume, for each point of contact along the contact circle, the rotor is being driven to rotate such that the linear velocity of the rotor at that point, defined from the rotor center by $\boldsymbol{r} = R\boldsymbol{e}_r$ (see Fig. 1(c)), is equal to the velocity of the substrate at the point of contact, $\dot{\boldsymbol{\xi}} = \dot{\eta}\boldsymbol{e}_x + \dot{\gamma}\boldsymbol{e}_z$. This implies the rotation of the rotor would be given by $\boldsymbol{\omega} \times \boldsymbol{r} = \dot{\boldsymbol{\xi}}$ if the action was only at this point. To find the angular velocity $\boldsymbol{\omega}$, we find $\boldsymbol{r} \times \dot{\boldsymbol{\xi}} = r^2\boldsymbol{\omega} - (\boldsymbol{\omega} \cdot \boldsymbol{r})\boldsymbol{r}$. Recognising that the only component of $\boldsymbol{\omega}$ that can be generated from enforcing a displacement constraint between the substrate and the rotor at the point must be perpendicular to $\boldsymbol{r}$, we are left with $\boldsymbol{r} \times \dot{\boldsymbol{\xi}} = |\boldsymbol{r} \cdot \boldsymbol{r}|\boldsymbol{\omega}$, easily solved for $\boldsymbol{\omega}$. Naturally, the angular velocity so produced varies around the contact circle of radius a, violating the pointwise constraint, and so we take the integral average of this pointwise velocity $\boldsymbol{\omega}$ over $\theta \in \{0, 2\pi\}$ for our estimate, as the rotor must do in response to the induced motion,

$$\omega_{\max} = \frac{1}{2\pi}\int_0^{2\pi} \frac{\boldsymbol{r} \times \dot{\boldsymbol{\xi}}}{|\boldsymbol{r} \cdot \boldsymbol{r}|}d\theta = \left(\frac{0.7\dot{\xi}\sqrt{R^2 - a^2}}{R^2}\right)\boldsymbol{e}_y; \quad (1)$$

the latter result as a consequence of assuming the spatial phase shift over the contact circle is negligible in which the radius of the hole $a < \lambda_{\mathrm{SAW}}$ where λ_{SAW} is the wavelength of
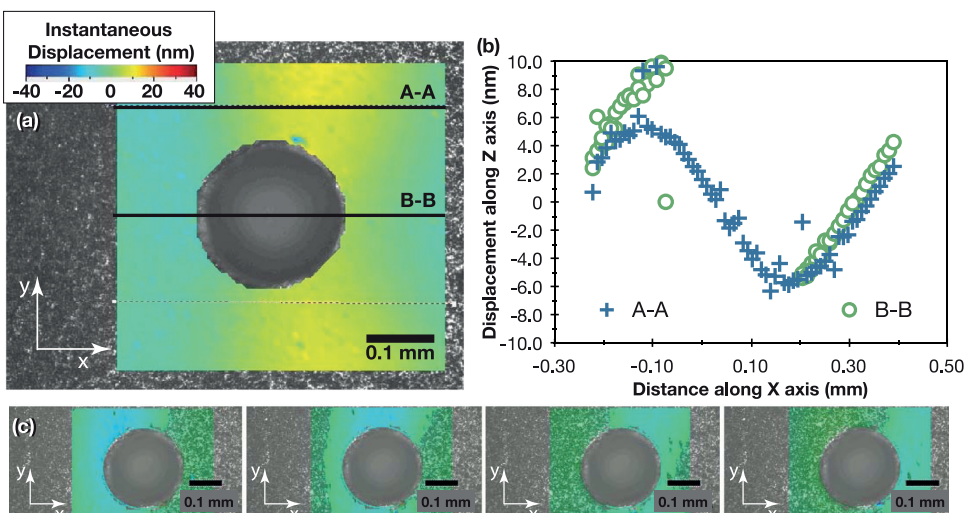

FIG. 2. (Color online) (a) SAW propagates left-to-right in the substrate, passing through the hole without substantial change as indicated by LDV measurement of the instantaneous z-polarized displacement, particularly in (b) comparison of the displacements along lines A–A and B–B, and (c) progressive images of the displacement, separated in time by 39 ns intervals (representing 1/8 of the wave period for 3.2 MHz) (enhanced online, along with demonstration of motor operation). [URL: http://dx.doi.org/10.1063/1.3662931.1]
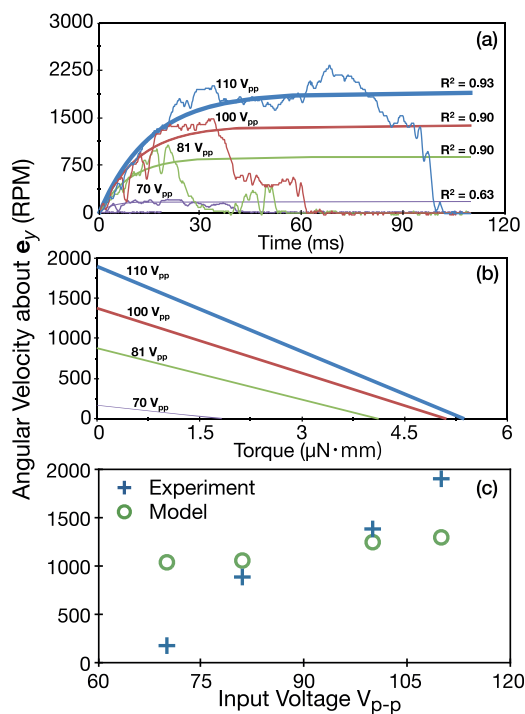
FIG. 3. (Color online) Angular velocity of the rotor with respect to (a) time and (b) torque of the motor obtained during operation with magnetic pre-load. The maximum speed achieved was approximately 1900 rpm, and the maximum torque achieved was 5.37 μN·mm using the weight of the rotor, approximately 41.1 μN, as the loading on the contact interface. Note the coefficient of determination, R^2, values is well above 0.5, permitting the use of Nakamura's method for estimating the torque-speed behaviour in (b). (c) Maximum model-predicted and experimentally measured rotor speeds in the system. The relatively poor comparison at low and high voltages is due to the complete absence of friction or stick-slip modelling in the very simple contact model, but the model does give an indication of the motor's output rotor speed without requiring substantial computations.

the SAW. Otherwise $\dot{\xi} = \dot{\xi}(\theta)$ and the integration may be more complex. With this assumption, most of the integrand is harmonic on $(0, 2\pi)$, including the contribution from the z-axis motion $\dot{\gamma} e_z$, and does not contribute to ω_{max}. The orientation of rotation is about the y axis with the rotor in contact with the substrate moving toward the SAW source, indicating a means to control the rotation axis by defining the direction of SAW incident upon the contact circle. Several IDTs placed about and pointed towards the contact can be used to change the rotation axis' orientation, as illustrated in the multimedia content provided with Fig. 2, though the axis will always remain parallel to the substrate surface.

The motor performance was measured using a laser tachometer (S-100 Z, Canon, Tokyo, Japan) and signal generator and amplifier (WF1946 and HSA4101, NF Corporation, Japan) as shown in Fig. 3. The comparison in this figure between the modeled and measured maximum rotor speed over a range of input voltages is provided; the weight of the rotor, approximately 41.1 μN in our system, was used as a very light preload, permitting rotor bouncing[26] in this early trial. The very simple theory offers a reasonable estimate for the rotor speed at intermediate voltages; considering the many assumptions underlying the very simple model, particularly in ignoring slip along the contact line, the rotor speed equation would be useful as a crude estimate. We modelled the motor's transient response as first-order lag system with good fit quality per Nakamura's method[27,28] to determine its torque and speed capabilities as shown in Fig. 3.

[1] B. Watson, J. Friend, and L. Yeo, Sens. Actuators, A **152**, 219 (2009).
[2] D. K.-C. Liu, J. Friend, and L. Yeo, Acoust. Sci. & Tech. **31**, 115 (2010).
[3] L. S. Fan, Y. C. Tai, and R. Muller, Sens. Actuators **20**, 41 (1989).
[4] J. Friend, L. Yeo, and M. Hogg, Appl. Phys. Lett. **92**, 014107 (2008).
[5] K. Asai and M. K. Kurosawa, Electron. Commun. Jpn. **88**(1), 37 (2005).
[6] M. Barbic, J. J. Mock, A. P. Gray, and S. Schultz, Appl. Phys. Lett. **79**, 1399 (2001).
[7] T. Kanda, A. Makino, T. Ono, K. Suzumori, T. Morita, and M. Kurosawa, Sens. Actuators A **127**, 131 (2006).
[8] A. Flynn, L. Tavrow, S. Bart, R. Brooks, D. Ehrlich, K. Udayakumar, and L. Cross, J. Microelectromech. Syst. **1**, 44 (1992).
[9] S. Biwersi, P. Gaucher, J. Hector, J. Manceau, and F. Bastien, Sens. Actuators, A **70**, 291 (1998).
[10] E. Hong, S. Trolier-McKinstry, R. Smith, S. Krishnaswamy, and C. Freidhoff, IEEE Trans. Ultrason. Ferroelectr. Freq. Control **53**, 697 (2006).
[11] K. Hashimoto, *Surface Acoustic Wave Devices in Telecommunications: Modelling and Simulation* (Springer, Berlin, Germany, 2000).
[12] R. White and F. Voltmer, Appl. Phys. Lett. **7**, 314 (1965).
[13] M. K. Kurosawa, M. Takahashi, and T. Higuchi, IEEE Trans. Ultrason. Ferroelectr. Freq. Control **43**, 901 (1996).
[14] K. Sakano, M. K. Kurosawa, and T. Shigematsu, Adv. Rob. **24**, 1407 (2010).
[15] J. Campbell and W. Jones, IEEE Transactions on Sonics Ultrason. **15**, 209 (1968).
[16] P. F. Bordui, D. H. Jundt, E. M. Standifer, R. G. Norwood, R. L. Sawin, and J. D. Galipeau, J. Appl. Phys. **85**, 3766 (1999).
[17] L. Cheng, G. Zhang, S. Zhang, J. Yu, and X. Shui, Ultrasonics **39**, 591 (2002).
[18] R. Shilton, N. Glass, P. Chan, L. Yeo, and J. Friend, Appl. Phys. Lett. **98**, 254103 (2011).
[19] R. P. Hodgson, M. Tan, L. Yeo, and J. Friend, Appl. Phys. Lett. **94**, 024102 (2009).
[20] J. Saito, J. Friend, K. Nakamura, and S. Ueha, Jpn. J. Appl. Phys. **44**, 4666 (2005).
[21] Y. J. Hsiao, T. H. Fang, Y. H. Chang, Y. S. Chang, and S. Wu, Mater. Lett. **60**, 1140 (2006).
[22] C. Tseng, J. Appl. Phys. **38**, 4281 (1967).
[23] S. Ueha and Y. Tomikawa, *Ultrasonic Motors—Theory and Applications*, Monographs in Electrical and Electronic Engineering Vol. 29 (Clarendon, Oxford, 1993).
[24] J. R. Friend, in *Proceedings of the 37th AIAA/ASME/ASCE/AHS/ASC Structures, Structural Dynamics, and Materials Conference and Exhibition* (American Institute of Aeronautics and Astronautics, 1996), Vol. 96, Paper No. 1452, pp. 1–15.
[25] J. Wallaschek, Smart Mater. Struct. **7**, 369 (1998).
[26] K.-C. Liu, J. Friend, and L. Yeo, Phys. Rev. E **80**, 046201 (2009).
[27] K. Nakamura, M. K. Kurosawa, H. Kurebayashi, and S. Ueha, IEEE Trans. Ultrason. Ferroelectr. Freq. Control **38**, 481 (1991).
[28] J. Friend, K. Nakamura, and S. Ueha, IEEE Trans. Ultrason. Ferroelectr. Freq. Control **52**, 1343 (2005).